Wind Energ. Sci. Discuss., https://doi.org/10.5194/wes-2017-62
Manuscript under review for journal Wind Energ. Sci.
Discussion started: 21 February 2018

eawe european academy of wind energy
Open Access WIND ENERGY SCIENCE DISCUSSIONS

Extending the life of wind turbine blade leading edges by reducing the tip speed during extreme precipitation events

Jakob I. Bech[1], Charlotte B. Hasager[1], Christian Bak[1]

[1]Department of Wind Energy, Technical University of Denmark, Roskilde, 4000, Denmark

Correspondence to: Jakob Ilsted Bech (jakb@dtu.dk)

Abstract. Impact fatigue caused by collision with rain droplets, hail stones and other airborne particles, also known as rain erosion, is a severe problem for wind turbine blades. Each impact on the leading edge adds an increment to the accumulated damage in the material. After a number of impacts the leading edge material will crack. This paper presents and supports the hypothesis that the vast majority of the damage accumulated in the leading edge is imposed at extreme precipitation condition events, which occur during a very small fraction of the turbines operation life. By reducing the tip speed of the blades during these events, the service life of the leading edges significantly increases from a few years to the full expected lifetime of the wind turbine. In the worst case at the cost of a negligible reduction of annual energy production (AEP) and in the best case with a significant increase in AEP.

1 Introduction

Leading edge erosion (LEE) is a severe challenge for the wind energy sector today (Keegan et al., 2013, Slot et al. 2015). Wind turbine operators report significant costs for inspection, maintenance, repair, and loss of production due to down time and reduced performance (Stephenson, 2011). LEE increases the surface roughness of blades and deteriorates the aerodynamic performance resulting in lower AEP during turbine operation (Zidane et al., 2016). The LEE issue has appeared as a consequence of the trend towards larger turbines with longer blades and higher nominal tip speeds (Keegan et al. 2013, Macdonald et al., 2016). As an example, recently 273 blades with less than 7 years in operation were refurbished at an offshore wind farm in the North Sea. Some of the blades were even removed and taken ashore for repair of damages due to LEE (Wittrup, 2015).

LEE is caused by a multitude of factors within the atmospheric environment and the leading edge structure. Efforts to understand rain-induced erosion include simulation (Blowers, 1969, Springer 1975, Sloth et al, 2015, Amirzadeh 2017) and laboratory testing (Bowden et al, 1964, Keegan et al. 2013). A thorough understanding of rain erosion of layered anisotropic polymer-based-structures like wind turbine blades is not yet available. However, it is clear, that several damage mechanisms are observed, and that the impact velocity is a governing factor as well as the amount of precipitation and the structure and materials of the leading edge.

Wind Energ. Sci. Discuss., https://doi.org/10.5194/wes-2017-62
Manuscript under review for journal Wind Energ. Sci.
Discussion started: 21 February 2018

The industrial standard for measuring the durability of leading edge strucures is the whirling arm rain erosion test (WA-RET) (ASTM G73-10, 2010, Liersch 2014). In the WA-RET the test specimens are mounted on a rotor spinning at high velocity in an artificially generated rain field. The rotor velocity, rain intensity and droplet size are carefully controlled, as impact velocity, droplet dimension and number of impacts are the governing factors for the magnitude of damage imposed on a given test specimen (Adler, 1999). The impact velocities of the accelerated tests are typically up to two times the tip speed of real blades, which may cause irrelevant failure modes. It should also be kept in mind, that the whirling arm test method does not necessarily reflect the real operating conditions. Rain droplet sizes and rain intensities vary, and impacts of hail stones and insects, global strain from blade flexing, temperature oscillations, UV radiation and long term exposure to moisture, chemicals and salt also add to the material degradation.

Blade- and turbine manufacturers as well as coating suppliers put effort to develop and implement leading edge protection structures that will last the expected lifetime of the turbines. Wind turbine (WT) operators put effort to define feasible inspection and service intervals and to repair damaged blades.

The latest developments in leading edge protection (LEP) applied to new turbines have yet to prove their durability in long term field conditions. Already installed turbines without the latest inventions in LEP are still vulnerable to erosion, and repairs made on site may have varying quality. Also, in order to reduce the torques and loads, it may be attractive to increase the tip speeds even further on future turbine designs. Consequently, alternative strategies of mitigation of LEE should be explored.

Such an alternative strategy is the reduction of the tip speed during highly erosive conditions (Wobben, 2003). It is likely to be feasible to extend the leading edge life by reducing the rotor speed during extreme precipitation events occurring at a very little fraction of the service life, but accounting for the majority of the erosion damage. This approach is also inspired by aerodynamic load control, where it is a common strategy to reduce the extreme loads caused by gusts and turbulence by pitching out the blades under these conditions. Such systems operate automatically in modern wind turbines. (IEC 61-400-1).

The objective of this paper is to present and support the hypothesis on mitigation of leading edge erosion by control of wind turbines during high impact rain events. In Sect. 2 some important aspects of leading edge erosion are presented with focus on liquid droplet impact stresses and fatigue. Section 3 presents an analysis of whirling arm rain erosion test data provided by Polytech A/S. The analysis includes introduction to block loading and a cumulative damage law. Section 4 presents precipitation parameters and their statistical occurrence, while Sect. 5 focuses on turbine control for reducing tip speed and includes control strategies with different loss of production vs. extension of life of blades. The discussion follows in Sect. 6 and conclusions are drawn in Sect. 7.

2 Rain erosion of leading edge

2.1 Droplet impact

Rain erosion is the consequence of multiple impacts stochastically distributed over the surface of the coated laminate. Each impact adds a damage increment to the accumulated damage. For rain and other air borne particles the accumulated damage is

Wind Energ. Sci. Discuss., https://doi.org/10.5194/wes-2017-62
Manuscript under review for journal Wind Energ. Sci.
Discussion started: 21 February 2018

eawe european academy of wind energy
Open Access WIND ENERGY SCIENCE DISCUSSIONS

a function of the number of impacts per unit area and the magnitude of each impact. This paper is limited to consider impact by liquid droplets only.

The magnitude of an impact of a droplet hitting perpendicular to the surface may be quantified by the kinetic energy (E_{kin})

$$E_{kin} = \frac{1}{2}mv^2 \text{ [J]} \quad (1)$$

where v is the velocity of the particle relatively to the surface and m is mass.

For detailed analysis the impact may be quantified by the contact stress field acting on the surface as a function of time during the impact. The contact stresses depend on the properties of the liquid, the properties of the target, the impact velocity and the size and shape of the droplet.

The impact of a spherical droplet immediately causes a normal pressure on the target surface at the initial point of contact. The contact area between the droplet and the solid expands radially at a velocity higher than the speed of sound in water. When the shock wave front reaches the edge of the droplet, a release jet is generated, and the pressure reduces to the stagnation pressure (Bowden 1964, Dear and Field, 1988).

The simplest expression for calculation of the initial contact pressure is the water hammer equation (Bowden 1961), which dates back to late 19th century and has since been explored by several researchers. It was derived for a column of liquid impacting a rigid surface, where a compression wave propagates from the contact into the liquid. The immediate contact pressure (p) may be calculated by

$$p = v\rho c \text{ [Pa]} \quad (2)$$

where c is speed of the compression wave and ρ is the density of the liquid. Accounting for the geometry of a spherical droplet, the contact angle increases as the contact area expands, and the peak pressure at the rim of the contact is analytically derived (Heymann, 1969) as

$$p = 3v\rho c \text{ [Pa]} \quad (3)$$

Taking into account the compliance of the solid, the pressure of impact between an elastic solid cylinder and a liquid jet (de Haller 1933) may be expressed as

$$p = v\frac{\rho_l c_l \rho_s c_s}{\rho_l c_l + \rho_s c_s} \text{ [Pa]} \quad (4)$$

where sub-script l is for liquid and s for solid. Later numerical modelling take into account an assumed spherical geometry of the droplet as well as the compliance of the target material (Adler 1995, Amirzadeh et al, 2017). These studies also show a pressure peak near the edge of the contact.

Real precipitation droplets falling through the atmosphere are not necessarily spherical. The aerodynamic forces distort the droplet to a burger bun - like shape. Larger droplets, d>6 mm, flatten out before splitting up (Fakhari 2009), while smaller droplets tend to merge and form larger droplets. The droplet geometry may be characterized by its ratio of vertical to horizontal

Wind Energ. Sci. Discuss., https://doi.org/10.5194/wes-2017-62
Manuscript under review for journal Wind Energ. Sci.
Discussion started: 21 February 2018

dimension (Gorgucci et al, 2006). Through a full rotation of 360 degrees the wind turbine blades are hitting the non-spherical droplets from all angles at different relative velocities. This again makes the impact scenario further complex.

2.2 Impact stresses, fracture and fatigue

A typical leading edge consists of a curved laminate of Glass Fiber-Reinforced Polymer (GFRP) with a relatively brittle polyurethane, polyester or epoxy –based coating. Many designs have a layer of putty or filler on the GFRP to make a smooth surface for the coating. Recent developments have added a top layer of elastomeric coating with good damping properties and high fracture toughness often referred to as leading edge protection or LEP.

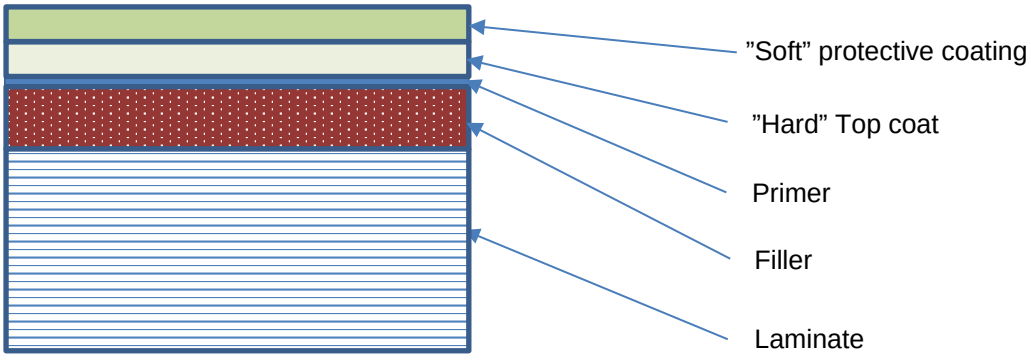

Figure 1: Example of leading edge structure.

An impact on the surface causes stress transients in the material. Stress waves propagate from the impact site into the coated composite (body waves) and along its surface (surface waves). Several stress components are active as functions of the time after the impact, the radial planar position and depth in the material (Woods 1968, Adler 1995). These stresses can activate different failure modes depending on the velocity of the impact, the size of the droplet and “the weakest link” in the leading edge structure.

For isotropic, homogenous, elastic materials ring shaped surface cracks due to Rayleigh waves is the common type of impact damage (Blowers 1969, Bowden, 1964). For many coated materials, this may also be the governing failure mechanism.

The body waves propagating perpendicular to the surface into the target material can lead to failure of either the coating or the substrate. The reflection of stress waves between the coating surface and the coating/substrate interface may also play a significant role for fatigue of the coated laminate (Springer 1974). Body waves may also cause delamination inside the laminate (Prayago 2011) and debonding of the coating (Cortés et al 2017).

A single droplet impact may cause instant damage, when the impact velocity is beyond the damage threshold velocity (DTV). For a given droplet size and set of material parameters, DTV was derived for brittle materials by a fracture mechanics approach, (Evans et al. 1980).

$$v_p^c = \sqrt[3]{\lambda \frac{(K_c^2 c)_t}{(r\rho^2 c^2)_p}} \text{ [m/s]} \quad (5)$$

Wind Energ. Sci. Discuss., https://doi.org/10.5194/wes-2017-62
Manuscript under review for journal Wind Energ. Sci.
Discussion started: 21 February 2018

where p denotes the impacting droplet and t denotes the target, r is the radius of the spherical droplet, K_c is the critical stress intensity factor, ρ is density c_t is the Rayleigh wave velocity of the target material and c_p is the speed of sound in water.

Repeated stresses below the static strength of a material may eventually cause failure due to cumulative fatigue damage (Minor 1945). Impacts below DTV may also add to the accumulated damage, that may eventually cause fracture (Springer 1975). For materials with a fatigue limit, like some metals, a fatique threshold impact velocity, below which no erosion will occur, may be defined as an analogy to the endurance limit found in fatigue testing (Heymann, 1969).

3 Empirical rain erosion test data

3.1 Analysis of rain erosion test data

An example of rain erosion test data was made available by Polytech A/S, see Fig. 2. The test specimen material is coated aluminum. The specimen has a length of 225 mm. In this test, the tangential velocity was 140 m/s at the tip and 110 m/s at the root of the specimen. The rain intensity was 30-35 mm/h and droplet sizes were ranging from 1 to 2 mm. (In the later calculations, for simplicity, it is assumed, that the rain intensity is 32.5 mm/h, the droplet diameter is uniform at 2 mm and the falling velocity of the droplets is 6 m/s). The test was stopped every 30 minutes for photography of the specimens, see Figure 2. The photographs are used to determine the progression of erosion. Here erosion is defined as visible removal of the top coat. The erosion initiates at the tip of the specimen, where velocity is highest, and propagates towards the root. Each position on the specimen corresponds to a certain tangential velocity. The data pairs of propagation of erosion and time are shown in Table 1 along with the corresponding local rotor velocities. The kinetic energy of each impact and the number of impacts per unit area are explained in Sect. 3.2.

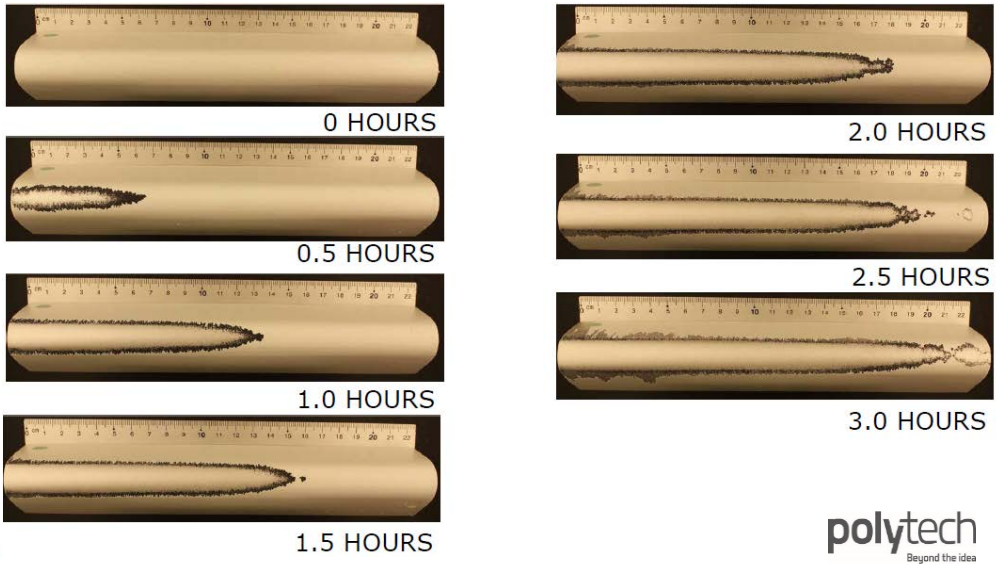

Figure 2: Whirling arm rain erosion test specimen photographed at 30 minutes intervals during 3 hours of testing.

Wind Energ. Sci. Discuss., https://doi.org/10.5194/wes-2017-62
Manuscript under review for journal Wind Energ. Sci.
Discussion started: 21 February 2018

Table 1: Erosion propagation as function of time

Test time [hrs]	Propagation of erosion [mm]	Accumulated rain [mm]	Local tangential rotor speed [m/s]	Kinetic energy [J]	Impacts/area to removed coating [cm^{-2}]
0.5	66	16	131	0.036	8.5E+03
1.0	135	33	122	0.031	1.6E+04
1.5	161	49	119	0.029	2.3E+04
2.0	182	65	116	0.028	3.0E+04
2.5	208	81	112	0.026	3.6E+04
3.0	228	98	110	0.025	4.3E+04

The data from Table 1 are plotted in a Wöhler diagram in Fig. 3, where, traditionally, the independent parameter, velocity, is plotted on the vertical axis and the dependent parameters, time or amount of rain before the coating is removed, are plotted on the horizontal axis of a semi logarithmic diagram. Such a representation of data is known from fatigue testing of materials (Miner, 1945; Ronold and Echtermeyer, 1996), where the number of load cycles causing failure is shown as a function of the magnitude of each load cycle (for example stress range). The fatigue data are often fitted to a power function as shown in Fig. 3.

It should be noted, that the time to removal of coating at position “i” is likely to be influenced by the adjacent erosion at position “i-1” as the damage progresses from an area of high velocity towards areas with lower velocity.

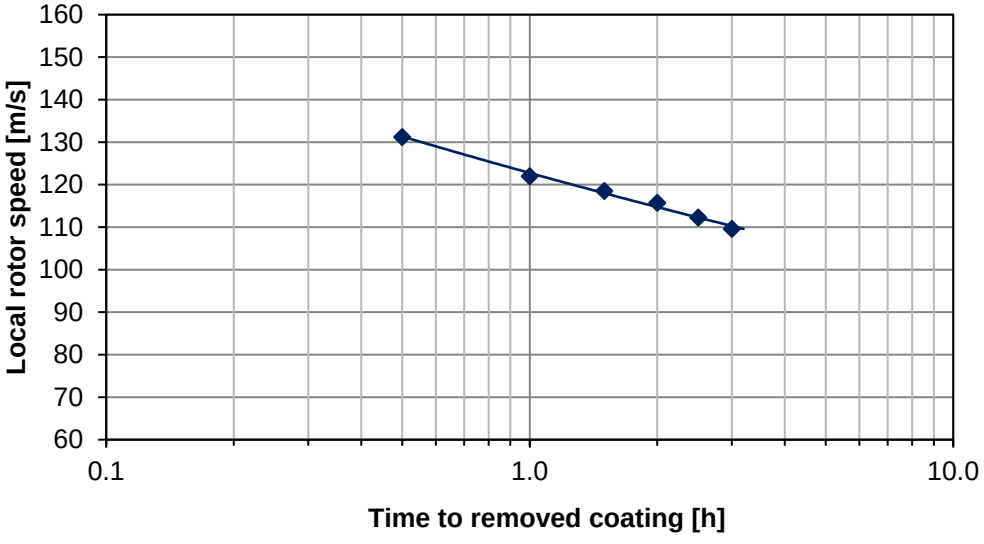

Figure 3: Rain erosion test data plotted as a Wöhler curve.

Wind Energ. Sci. Discuss., https://doi.org/10.5194/wes-2017-62
Manuscript under review for journal Wind Energ. Sci.
Discussion started: 21 February 2018

eawe european academy of wind energy
Open Access WIND ENERGY SCIENCE DISCUSSIONS

3.2 Generalizing empirical values

Exactly how the droplet sizes and velocities influence the damage is unknown. It obviously depends on several factors including material configuration: properties of hard coating, of laminate, of elastomer coating, thicknesses, interfaces and various failure modes. We now take the hypothesis that the kinetic energy of each impact characterizes the magnitude of each impact, and the number of impacts per cm^2 corresponds to the number of cycles in a fatigue test.

In a rain field with assumed spherical droplets with uniform diameter and constant falling velocity the relative volume of water (V) is given by

$$V = \frac{I_r}{v_r} \quad [-] \tag{6}$$

where I_r is rain intensity and v_r is falling velocity.

The number of droplets pr volume (N) can be expressed as

$$N = 6\frac{I_r}{v_r \pi D^3} \quad [\mathrm{m}^{-3}] \tag{7}$$

where D is droplet diameter.

An object travelling through a rain field is hit by droplets in a stochastic manner across its surface. Assuming that the droplets are distributed evenly in space, and their velocity is negligible compared to the speed of the object, the number of impacts pr unit projected area pr time, F, can be expressed as

$$F = N * v_t \quad [\mathrm{s}^{-1}\mathrm{m}^{-2}] \tag{8}$$

The kinetic energy (E_k) of each impact is

$$E_k = \frac{1}{12}\rho\pi D^3 v_t^2 \quad [\mathrm{J}] \tag{9}$$

Now, the test data from Table 1can be presented as the number of impacts pr unit area (N_{EI}) as a function of the kinetic energy of each impact before visible erosion, see Figure 4. The data can be fitted to a power function:

$$N_{Ei} = c * E_k^{-m} \quad [\mathrm{m}^{-2}] \tag{10}$$

A power function fit of the test data in Table 1 to Eq. (10) gives c=18 and m=4.63

We now take the additional hypothesis, that the incremental damage is a function of the impact energy only, and that Eq. (10) holds for different droplet diameters.

Combining Eq. (9) and Eq. (10), the fatigue life can be expressed as a function of the impact velocity and the droplet diameter

$$N_{Ei} = c * \left(\frac{1}{12}\rho\pi D^3 v_t^2\right)^{-m} \tag{11}$$

Now, applying Eq. (11), Wöhler curves can be drawn for different droplet diameters as shown in Fig. 5.

Wind Energ. Sci. Discuss., https://doi.org/10.5194/wes-2017-62
Manuscript under review for journal Wind Energ. Sci.
Discussion started: 21 February 2018

Back calculating from impacts per area to millimeters of accumulated rain, one gets the Wöhler curves for accumulated rain to remove the coating as a function of the rotor velocity for different droplet diameters as shown in Figure 6.

Given the assumptions and extrapolation it is obvious that droplet size is important and not just the amount of rain.

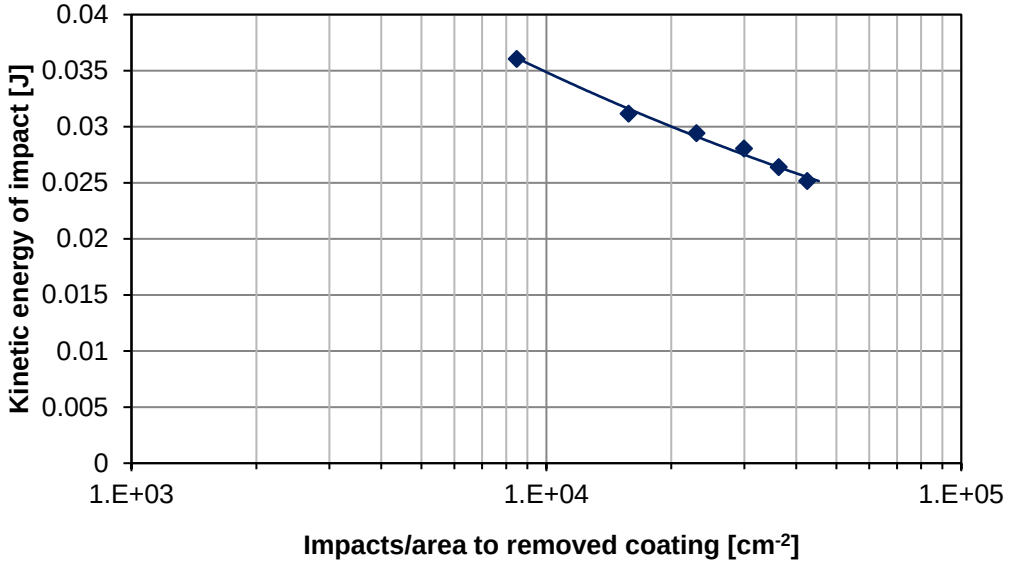

Figure 4: Rain erosion test data plotted as a Wöhler curve: impacts per unit area to failure as function of the kinetic energy for each impact

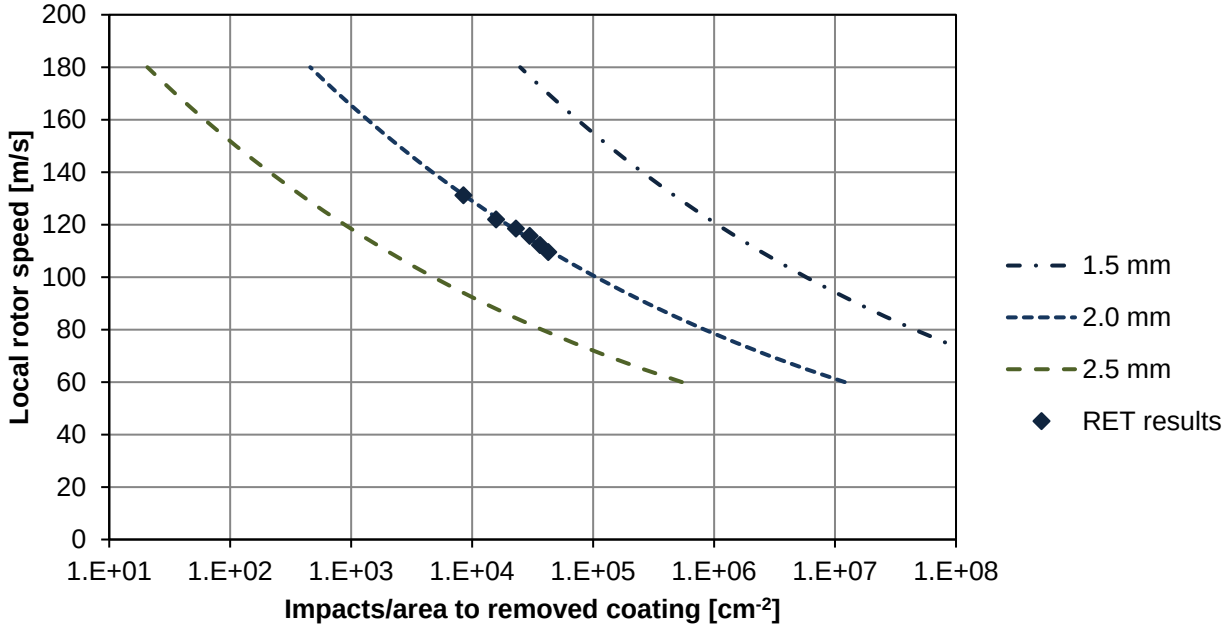

Figure 5: Wöhler curves for droplet diameters of 1.5, 2.0 and 2.5 mm

Wind Energ. Sci. Discuss., https://doi.org/10.5194/wes-2017-62
Manuscript under review for journal Wind Energ. Sci.
Discussion started: 21 February 2018

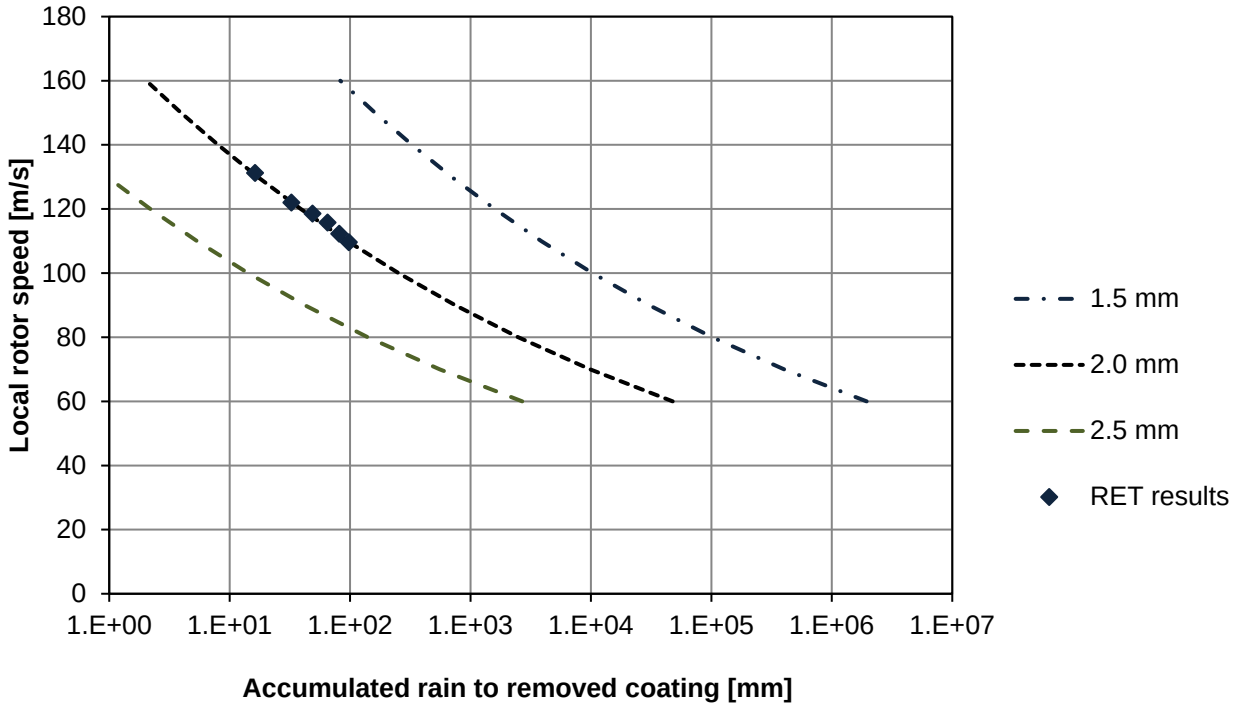

Figure 6. Expected accumulated rain to remove coating as function of rotor speed for droplet diameters of 1.5, 2.0 and 2.5 mm

3.3 Block loading and cumulative damage laws

Each point on the Wöhler curve in Fig. 3 corresponds to a test run at constant conditions (rain intensity, droplet size, local rotor speed). However, most structures designed for cyclic loads are subject to varying load intensities in service. For instance a wind turbine blade will see a spectrum of wind speeds, gusts and turbulence over its lifetime. Likewise a leading edge will be impacted with rain of varying droplet sizes and intensities, changing impact velocities and other particles like hail stones. To account for variable conditions fatigue loading, different rules have been proposed for accumulation of damage in composites (Brøndsted et al. 1997). The most popular and easy to use, though not always correct, is the linear Palmgren-Miner rule. Accumulated damage (M) is given by

$$M = \sum_{i=1}^{j} \frac{n_i}{N_i} \tag{12}$$

Here i is load level number, n_i is number of cycles at level i, N_i is cycles to failure at level i in a test and j is number of load levels.

The Palmgren-Miner rule will be applied later to predict the fatigue life of a leading edge based on the presented RET data and rain statistics. Given a load time history and Wöhler curves for different loading conditions, it is possible to use Miner's rule to determine the accumulated damage or fatigue life of a structure or material.

Wind Energ. Sci. Discuss., https://doi.org/10.5194/wes-2017-62
Manuscript under review for journal Wind Energ. Sci.
Discussion started: 21 February 2018

4 Precipitation

Estimation of the potential erosion caused by rain at specific wind farm sites has to be based on information on precipitation, wind speed and turbine characteristics such as tip speed. Wind speeds at wind farm sites are usually known from wind resource assessment during the planning phase and on site wind observations during the operational phase. In contrast, precipitation is not standard observation, neither for planning, nor for operation of wind farms.

Early studies on raindrop size distribution (Best, 1950; Mason and Andrews, 1960) showed rain intensity and raindrop size to relate to each other for a wide range of climate conditions. Fig. 7 shows the probability density function as a function of raindrop diameter based on Best (1950).

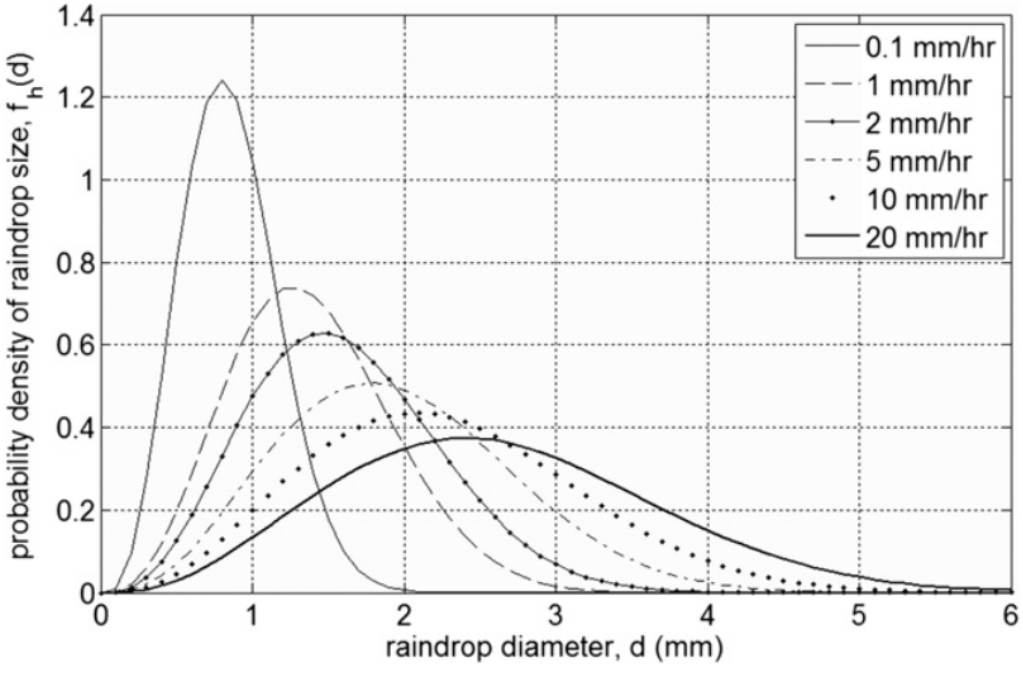

Figure 7: Raindrop size distribution through a horizontal plane with the rain fall intensity as a parameter (from Kubilay et al., 2013, based on Best, 1950).

Rain intensity (or rate) is typically measured as mm/h. Rain intensity varies a lot with time. The shorter the interval of measurement, the more detailed is the picture of variation. For a convective rain event the rain intensity at 1 minute intervals can be more than 10 times the intensity measured at 60 minutes intervals. Based on disdrometer observation during thunderstorms in New Jersey, USA, it was shown that raindrop size distribution and rainfall intensity in heavy rain can be described from a Gamma distribution (Smith et al., 2009). Similar results are found in tropical rainfall during the monsoon season in Malaysia (Hong et al., 2015). Precipitation measured by disdrometers at locations across the globe from Australia and Asia to Europe and America confirm the relationship between rain intensity and raindrop size distribution (Bringi et al., 2003). Interestingly, Bringi et al. (2013) distinguish between convective ‘maritime’ and convective ‘continental’ raindrop size

Wind Energ. Sci. Discuss., https://doi.org/10.5194/wes-2017-62
Manuscript under review for journal Wind Energ. Sci.
Discussion started: 21 February 2018

distributions with the first being characterized by a lower concentration of larger-sized drops as compared to the latter. The generalization on average rainfall rate and percentage of time of exceedance for different rain climates is shown in Fig. 8.

Precipitation varies much across the globe. Mean annual precipitation and the monthly mean precipitation during the driest and wettest months are used in the Köppen-Geiger climate classification (Peel et al., 2007). The climatological standard normal covers 30 years according to the World Meteorological Organization. The mean annual precipitation normal is based on local network station records on land and varies much spatially. Table 2 lists data from Scandinavia, the UK, Europe and the World. The wettest place on Earth is said to be in India with 11.871 mm per year (Source: World Atlas).

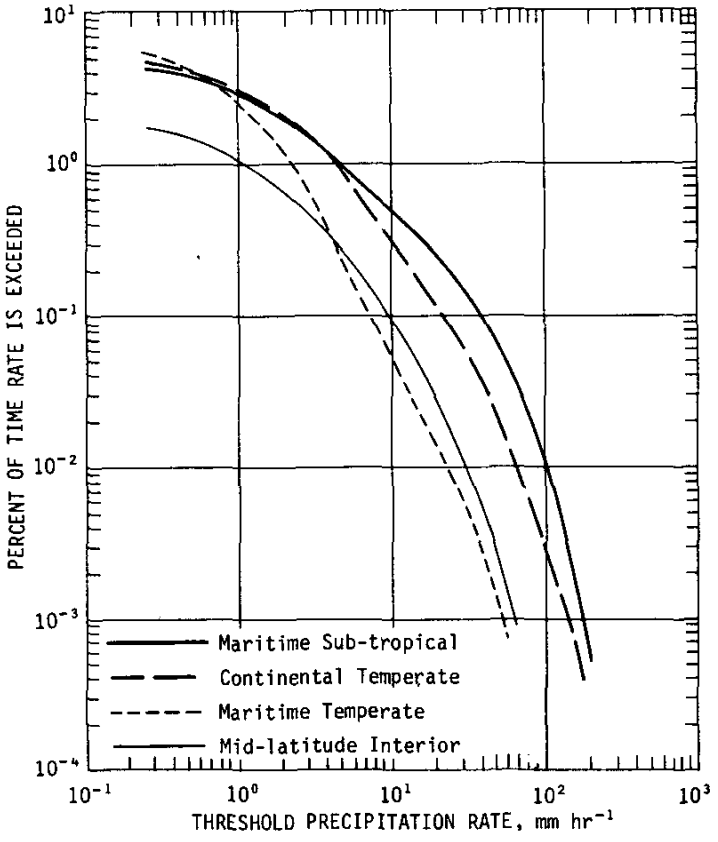

G. 5. Average rainfall rate-frequency relationships for four rain climates.

Figure 8: Average rainfall rate-frequency relationships for four rain climates (Jones and Sims, 1978) ©American Meteorological Society. Used with permission.

Wind Energ. Sci. Discuss., https://doi.org/10.5194/wes-2017-62
Manuscript under review for journal Wind Energ. Sci.
Discussion started: 21 February 2018

Table 2: Mean annual precipitation ranges over land in selected countries, Europe and the World.

Country	Range in mm	Period	Source
Denmark	<500 to >900	1961-1990	Frich et al. 1997
Finland	400 to >800	1971-2000	FMI
Norway	<300 to >4.000	1961-1990	Met.no
Sweden	400 to > 2.000	1961-1990	SMHI
UK	<400 to > 3.000	1981-2010	Met Office
Europe	<300 to > 4.000	n.a.	http://i.imgur.com/kEJhdOK.jpg; Panagos et al., 2015 (their Fig.1)
World	<50 to > 11.000	n.a.	WorldClim; Climate-Charts.com;GPCC

Precipitation over the ocean is mapped mainly by Earth observing satellites and to lesser degree based on sparse observations from ships and weather stations on small islands. The annual precipitation during the years 1998 to 2011 observed by the Tropical Rainfall Microwave Mission (TRMM) between latitudes 40°N and 40°S is shown in Fig. 9. The spatial resolution is 0.25° by 0.25°. Annual rainfall up to 7300 mm is noted in some tropical regions over ocean. Over land the TRMM map shows dry and wet regions corresponding to precipitation maps based on weather stations.

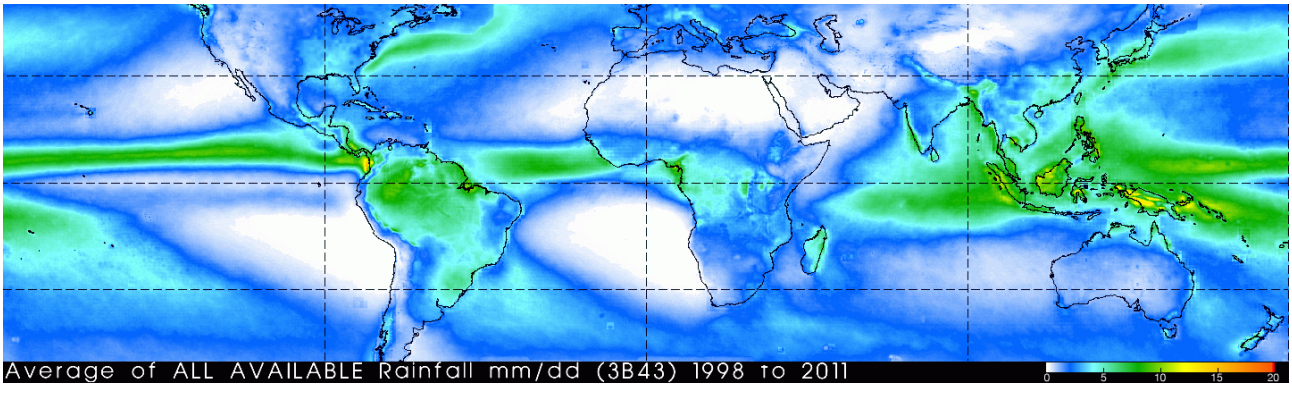

Figure 9. Average rainfall measured by TRMM from 1998 to 2011. Source: NASA.

The global precipitation map covering the years 1988 to 2004 is shown in Fig. 10. This map is based on the Special Sensor Microwave Imager, GOES precipitation index, outgoing longwave precipitation index, rain gauges, and sounders on NOAA satellites (Source: GPCP). The spatial resolution is 2.5° by 2.5°. The map shows, that annual precipitation is above 3300 mm per year over the ocean in some tropical regions. It may be noted that this spatial resolution does not resolve details. The maps for Scandinavia, the UK, Europe and the World listed in Table 2 do not cover the sea. TRMM only covers between 40°N and 40°S. Thus a map of the 30 year mean annual precipitation in the Northern European Seas where the majority of offshore wind farms are located is not available (to the knowledge of the authors).

Wind Energ. Sci. Discuss., https://doi.org/10.5194/wes-2017-62
Manuscript under review for journal Wind Energ. Sci.
Discussion started: 21 February 2018

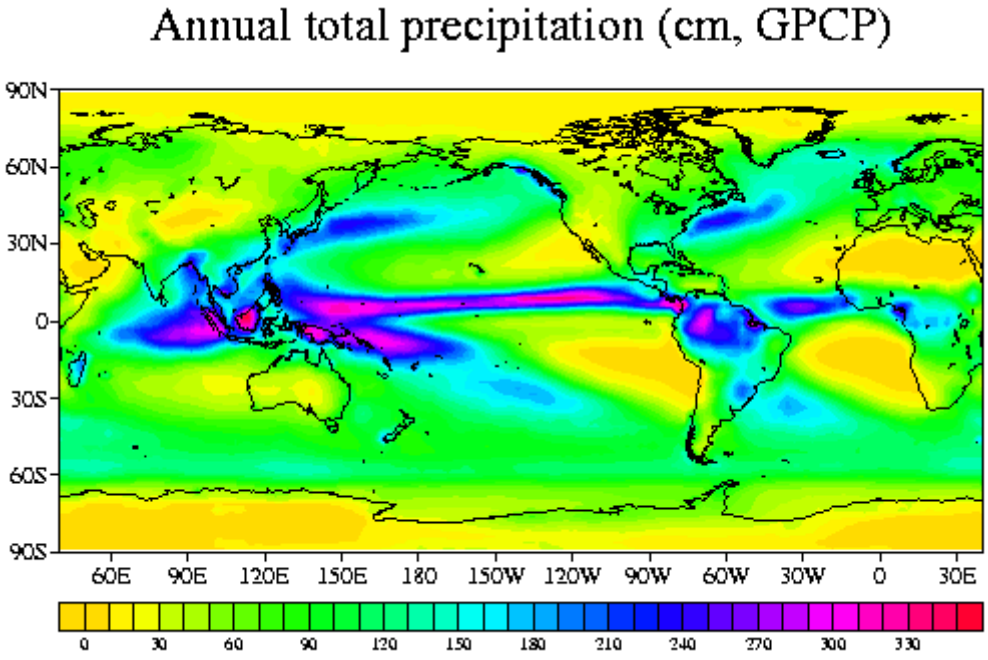

Figure 10: Average rainfall measured by several satellites, sounders and rain gauges combined for the years 1988 to 2004. Source: GPCP.

The objective to estimate the potential erosion caused by rain at specific wind farm sites is obviously more challenging at sea than at land due to the limited available precipitation data. Over land the rainfall erosivity for soil degradation has been assessed from weather station data (Panagos et al., 2015; Panagos et al. 2017). It is based on the Revised Universal Soil Loss Equation (RUSLE) method (Naipal et al. 2015). Rainfall erosivity is modelled as a function of the kinetic energy of rain, the maximum intensity of rainfall, the cumulative rainfall, the soil properties and the slopes of terrain. The map on rainfall erosivity in Europe at 500 m spatial resolution assessed by European Soil Data Centre (ESDAC) is shown in Fig. 11 (Panagos et al., 2015). A comprehensive precipitation database is established (Source: ESCAC; Panagos et al., 2015; Panagos et al. 2017). This database would be valuable for the production of a rain erosion map for wind turbines where precipitation, wind speed and turbine characteristics such as tip speed would be input.

For offshore wind farms the leading edge life is roughly half of what is observed on land, likely due to rain and wind but also ocean salinity and marine air composition (private communication). The wind turbine blades offshore need inspection and repair during life time. The access to offshore wind farms is dependent upon suitable weather windows and the logistics cost is higher when more waiting time occur (Poulsen et al. 2017). During repair with leading edge protection on offshore blades the weather window require benign wind and wave plus additionally air temperatures above 15°C, relative humidity <80% and no warning for thunderstorm and lightning. In the Northern European Seas this limits repair campaigns to the summer period. It may be valuable to assess the likelihood of suitable weather windows, in addition to the wind resource and the potential rain erosion for improved overall assessment of life time cost for offshore wind farms.

Wind Energ. Sci. Discuss., https://doi.org/10.5194/wes-2017-62
Manuscript under review for journal Wind Energ. Sci.
Discussion started: 21 February 2018

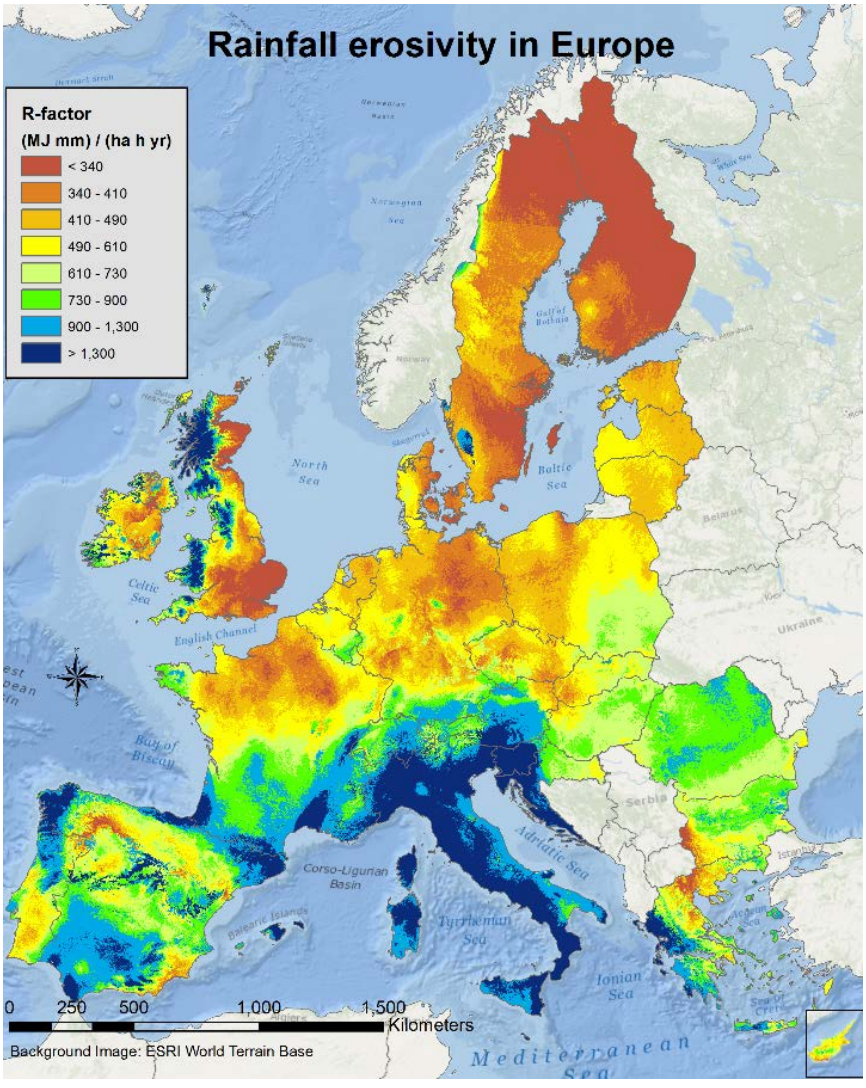

Figure 11: Rainfall erosivity in Europe at 1-km gric cell resolution. Source: Panagos et al., 2015. Creative Commons Attribution-NonCommercial-No Derivatives License (CC BY NC ND), https://doi.org/10.1016/j.scitotenv.2015.01.008

5 Turbine control for reducing tip speed

Leading edge erosion causes an increase in surface roughness and thereby an increase in the boundary layer thickness over the airfoils on the blade when it is operating. The increased boundary layer thickness results in a reduced aerodynamic performance. The higher the surface roughness, the thicker the boundary layer and the more reduction of the aerodynamic performance. To investigate the influence of the erosion on the aerodynamic performance, aerodynamic rotor computations were carried out for a Vestas V52 wind turbine with a modified control compared to an original Vestas V52, to determine the influence on the annual energy production (AEP). First, the method is described, and then the results are shown.

Wind Energ. Sci. Discuss., https://doi.org/10.5194/wes-2017-62
Manuscript under review for journal Wind Energ. Sci.
Discussion started: 21 February 2018

5.1 Methods

5.1.1 The wind turbine

The investigation was carried out as simulations on the Vestas V52 850 kW pitch regulated variable speed wind turbine that was erected at the DTU Risø Campus during the summer of 2015, Table 3. This wind turbine was investigated because data was available. However, parts of the input were modified, e.g. the rotational speed to make it consistent with the higher tip speeds that modern wind turbines are designed with. The size of the wind turbine is somewhat smaller than the volume of wind turbines installed during the last decade, but the losses in annual energy production is with relative considerations similar.

Table 3: Data for the Vestas V52 wind turbine.

Technical data for the Vestas V52-850kW	
Power regulation	Variable speed / variable pitch
Number of blades	3
Rotor diameter	52 [m]
Hub height	44 [m]
Maximum rotor speed	33 rpm

5.1.2 Control of the wind turbine

The wind turbine control is of the pitch regulated variable speed type. The maximum tip speed is set to 90m/s, and is thereby greater than the tip speed of an original Vestas V52 wind turbine. Compared to common control strategies, this wind turbine is assumed to be equipped with a sensor measuring the rain intensity and/or the droplet size. Apart from a reference case where it is assumed that there is no erosion, six different control strategies are investigated based on the model for expected lifetime for the blade leading edge:

- Control strategy 1 with expected life time of 1.6 years
- Control strategy 2 with expected life time of 10.4 years
- Control strategy 3 with expected life time of 24.4 years
- Control strategy 4 with expected life time of 53.9 years
- Control strategy 5 with expected life time of 106.5 years
- Control strategy 6 with expected life time of infinite many years

The results of the five first control strategies are shown in Table 4 to Table 8**.**. Control strategy 6 is a reference where it is assumed that no erosion will occur. The control strategies are calculated based on precipitation data from maritime temperate climate from Fig. 8. The droplet sizes for each rain intensity are assumed based on Fig. 7 and extensive extrapolation as described in Sect. 3 of the RET data shown in Table 1**.**. The control strategies are based on an assumed behavior that there is correspondence between the surface roughness height and the aerodynamic performance. Thus, there are elements in this

Wind Energ. Sci. Discuss., https://doi.org/10.5194/wes-2017-62
Manuscript under review for journal Wind Energ. Sci.
Discussion started: 21 February 2018

eawe european academy of wind energy
Open Access WIND ENERGY SCIENCE DISCUSSIONS

analysis that are not documented, but are based on qualified assumptions. However, the numbers are believed to be sufficiently realistic to demonstrate the potential of erosion control.

The results in Table 4 are based on data in Fig. 7 and Fig. 8 of assumed rain intensity durations and constant droplet size for each rain intensity. The first row in Table 4 is explained: the probability of rain intensity of 20 mm/hour with 2.5 mm droplets is around 0.02% or 1.8 hour pr year. At this rain intensity the total lifetime before failure at 90 m/s is around 3.5 hours. The fraction of damage relative to failure at this level is 51%. Summing up the fractions of damage at the five different rain intensities gives 0.64 or 64%. The calculated blade life at these conditions is therefore 1/0.64=1.6 year.

The results in Table 5 shows the effect of reducing the tip speed to 70 m/s and 80 m/s, respectively, at the two heaviest rain intensities. Because of the reduction of tip speed the blade life is extended to 10.4 years. In Table 6 to Table 8 the results are shown where further increases in the lifetimes were obtained.

Table 4: Calculation of the life time of the blade leading edge with no reduction of the tip speed. Control strategy 1.

Rain intensity [mm/hr]	Droplet size [mm]	Percent of time [%]	Hours pr year [hrs/year]	Blade tip speed [m/s]	Hours to failure [hrs]	Fraction of life spent pr year [%]
20	2.5	0.02	1.8	90	3.5	51
10	2.0	0.1	8.8	90	79	11
5	1.5	1	88	90	3606	2.4
2	1.0	3	263	90	745710	0.0
1	0.5	5	438	90	2830197826	0.0
				Sum of fractions [%]:		64
				Expected life [years]:		1.6

Table 5: Calculation of the life time of the blade leading edge with reduction of the tip speed to 70m/s and 80m/s, respectively: Control strategy 2

Rain intensity [mm/hr]	Droplet size [mm]	Percent of time [%]	Hours pr year [hrs/year]	Blade tip speed [m/s]	Hours to failure [hrs]	Fraction of life spent pr year [%]
20	2.5	0.02	1.8	70	46	3.8
10	2.0	0.1	8.8	80	263	3.3
5	1.5	1	88	90	3606	2.4
2	1.0	3	263	90	745710	0.0
1	0.5	5	438	90	2830197826	0.0
				Sum of fractions [%]:		9.6
				Expected life [years]:		10.4

Wind Energ. Sci. Discuss., https://doi.org/10.5194/wes-2017-62
Manuscript under review for journal Wind Energ. Sci.
Discussion started: 21 February 2018

eawe european academy of wind energy
Open Access WIND ENERGY SCIENCE DISCUSSIONS

Table 6: Calculation of the life time of the blade leading edge with reduction of the tip speed to 60m/s and 70m/s, respectively: Control strategy 3

Rain intensity [mm/hr]	Droplet size [mm]	Percent of time [%]	Hours pr year [hrs/year]	Blade tip speed [m/s]	Hours to failure [hrs]	Fraction of life spent pr year [%]
20	2.5	0.02	1.8	60	222	0.8
10	2.0	0.1	8.8	70	1036	0.8
5	1.5	1	88	90	3606	2.4
2	1.0	3	263	90	745710	0.0
1	0.5	5	438	90	2830197826	0.0
				Sum of fractions [%]:		4.1
				Expected life [years]:		24

Table 7: Calculation of the life time of the blade leading edge with reduction of the tip speed to 60m/s, 70m/s and 70m/s, respectively: Control strategy 4

Rain intensity [mm/hr]	Droplet size [mm]	Percent of time [%]	Hours pr year [hrs/year]	Blade tip speed [m/s]	Hours to failure [hrs]	Fraction of life spent pr year [%]
20	2.5	0.02	1.8	60	222	0.8
10	2.0	0.1	8.8	70	1036	0.8
5	1.5	1	88	70	47514	0.2
2	1.0	3	263	90	745710	0.0
1	0.5	5	438	90	2830197826	0.0
				Sum of fractions [%]:		1.9
				Expected life [years]:		54

Table 8: Calculation of the life time of the blade leading edge with reduction of the tip speed to 55m/s, 65m/s and 70m/s, respectively: Control strategy 5

Rain intensity [mm/hr]	Droplet size [mm]	Percent of time [%]	Hours pr year [hrs/year]	Blade tip speed [m/s]	Hours to failure [hrs]	Fraction of life spent pr year [%]
20	2.5	0.02	1.8	55	541	0.3
10	2.0	0.1	8.8	65	2215	0.4
5	1.5	1	88	70	47514	0.2
2	1.0	3	263	90	745710	0.0
1	0.5	5	438	90	2830197826	0.0
				Sum of fractions [%]:		0.9
				Expected life [years]:		107

Not to overload the drivetrain it was ensured not to exceed the maximum rated shaft torque. Thus, when operating at different maximum tip speeds the wind turbine had to operate at different rated power:

- 90m/s: 850kW
- 80m/s: 760kW
- 70m/s: 660kW
- 65m/s: 615kW
- 60m/s: 570kW
- 55m/s: 520kW

Even though the wind turbine experience heavy rain and have to reduce the tip speed, the wind turbine will produce some power; thus only part of the potential power is lost. By using the erosion safe mode the repair and loss in production due to leading edge erosion will be reduced.

5.1.3 Determination of the loss in annual energy production

The prediction of the rotor performance was based on a design tool, HAWTOPT, for multi point wind turbine design, which uses numerical optimization. The tool is basically a Blade Element Momentum (BEM) code with the ability also to compute e.g. energy production, and with the further ability also to optimize the control using numerical optimization. HAWTOPT was used to calculate the aerodynamic performance of the Vestas V52 rotor given different sets of airfoil characteristics corresponding to different degrees of erosion. For further information about HAWTOPT, see Fuglsang et al. (2001). HAWTOPT calculated the annual energy production based on the power curve that is a result of the BEM computation and a Weibull distribution, where the mean wind speed is varying, so that A=7m/s, 8m/s and 9m/s, and where the shape is constant, C=2. The airfoil characteristics for the blades in terms of lift coefficients, drag coefficients and moment coefficients as a function of angles-of-attack were predicted as described in the Sect. 5.1.4.

5.1.4 Method for derivation of aerodynamic airfoil data

Flow computations using *XFOIL* (version 6.1) developed by Drela (1989) were carried out in the angle-of-attack range between -20° to 20°, because wind tunnel tests were not available for all airfoil sections on the blade. In the computations both free transition modeled by the e^n method and forced transition (x/c=0.1% at suction side and x/c=10% at the pressure side) were used. In the e^n model the value n=7 was used because this corresponds to around a turbulence intensity of 0.1%, which is common for high quality wind tunnels and because this value has shown to predict the transition point position well compared to tunnel tests and atmospheric flow.

For angles of attack in the range [-180°;-45°] and [45°;180°] it is assumed that the airfoils respond as flat plates and therefore can be described by the following functions irrespectively of clean or contaminated surfaces: $c_l=2\cos(\alpha)\sin(\alpha)$, $c_d=1.3\sin^2(\alpha)$ and $c_m=-\sin(\alpha)/4$

For angles of attack in the range [-45°;-20°] and [20°;45°] the data is interpolated between the data point at α=±20° based on the predictions by XFOIL and the data point at α=45° based on the assumptions of flat plate.

Wind Energ. Sci. Discuss., https://doi.org/10.5194/wes-2017-62
Manuscript under review for journal Wind Energ. Sci.
Discussion started: 21 February 2018

Finally, the airfoil characteristics (except for the cylinder part) are 3D corrected according to Bak *et al.(2006).* The 3D correction is carried out in the range [0;45°], so to connect data in this range to the range [45°;180°], the data points between α=45° and α=60° for airfoil thicknesses t/c=24%, 30% and 36% have been changed to avoid abrupt changes in the airfoil characteristics.

An example of a set of derived data is shown in Figure , where the airfoil characteristics for the outer part of the blade, the airfoil with a relative thickness of 15%, are seen. To the left, plots of lift coefficient, c_l, as a function of drag coefficient, c_d, is seen. To the right lift coefficient, c_l, as a function of angle of attack is seen. The blue curves show the performance for perfectly clean airfoils, whereas the orange curves show the performance for airfoils with heavy Leading Edge Roughness (LER) that corresponds to full blade life for the airfoil as stated in Table 4 to 8. An example of an airfoil performance with 60% of heavy LER are shown with the green curves. The green curves are simple interpolations between the curves for perfectly clean airfoils and airfoils with heavy LER.

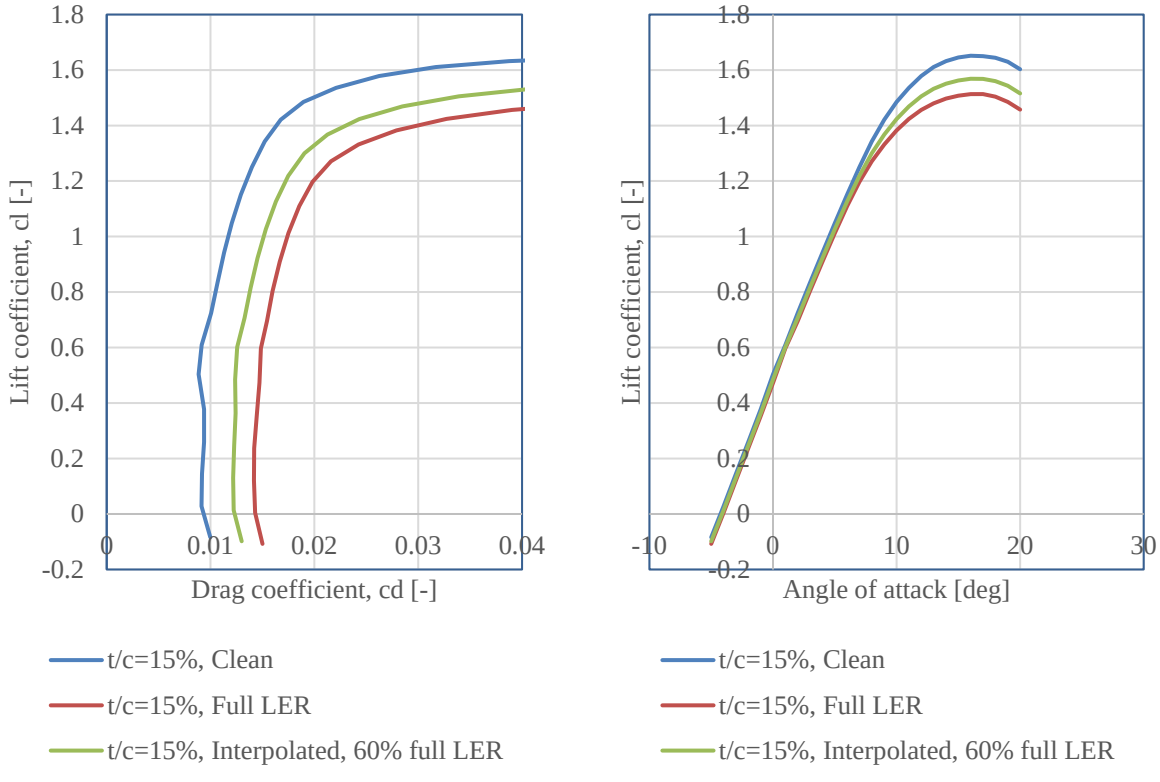

Figure 12: Aerodynamic airfoil characteristics of the airfoils on the outer part of the blade in case of a completely clean blade, a blade with severe leading edge roughness (erosion) and a blade with leading edge roughness corresponding to 60% severe leading edge roughness. Left: Lift coefficient, cl, as a function of drag coefficient, cd. Right: Lift coefficient, cl, as a function of angle-of-attack, AOA.

Wind Energ. Sci. Discuss., https://doi.org/10.5194/wes-2017-62
Manuscript under review for journal Wind Energ. Sci.
Discussion started: 21 February 2018

Power curves for different levels of LER are shown in Fig. 13, where the clean blade, the blade with full LER and some of the intermediate roughness levels are reflected. Thus, the intermediate roughness levels represent the corresponding lifetime, so e.g. 20% of full LER corresponds to 20% of the lifetime. This correspondence is not documented and is therefore a postulate that is however based on experience. In the analysis, roughness levels with steps of 10% difference are used.

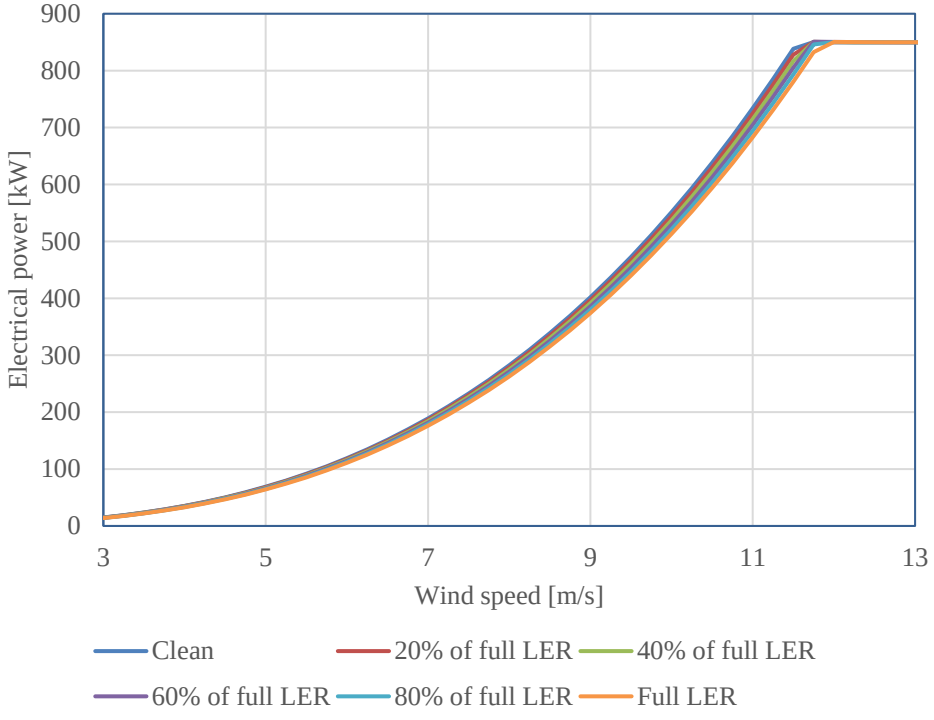

Figure 13: Simulated power curves for the Vestas V52 for different leading edge roughness levels.

Power curves for different types of control are shown in Fig. 14. The plot shows how the power curves change when the tip speed is reduced, not to overload the shaft torque. It shows that the power curves are almost identical from wind speeds of 3m/s to 9m/s. Thus, reduction of the rated power will influence the production for wind speeds greater than 9m/s.

Wind Energ. Sci. Discuss., https://doi.org/10.5194/wes-2017-62
Manuscript under review for journal Wind Energ. Sci.
Discussion started: 21 February 2018

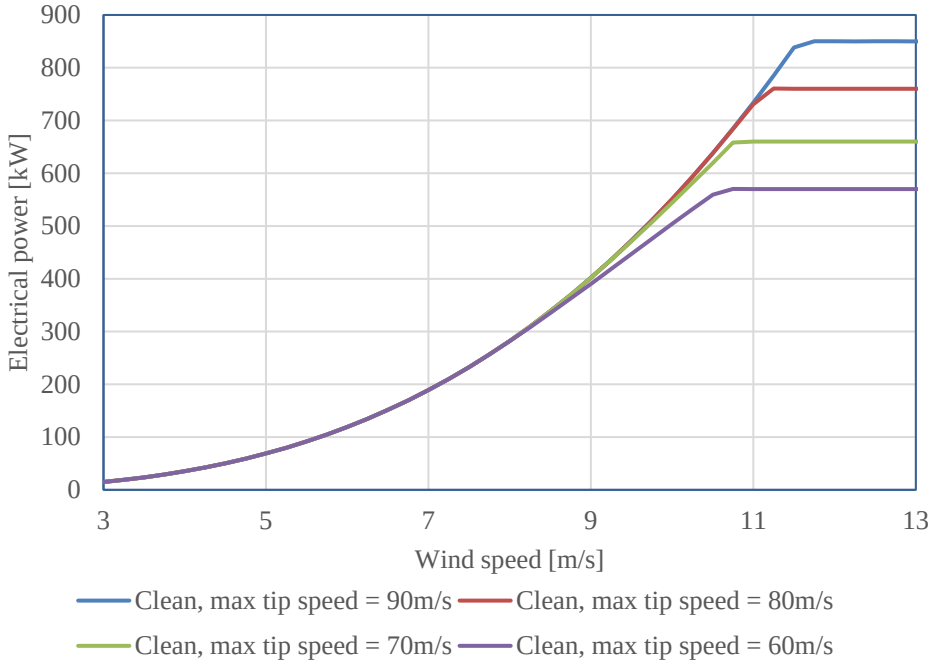

Figure 14: Simulated power curves for the Vestas V52 for different maximum tip speeds.

5.1.5 Cost of operation and maintenance

Prices for the energy and the cost for inspection and repair can vary. In the analysis of the cost of using erosion safe control, the following cases are used:

- Energy price:
  - 50 €/MWh
  - 250 €/MWh
- Inspection cost:
  - 500 €/rotor
  - 1500 €/rotor
- Repair cost
  - 10000 €/rotor
  - 20000 €/rotor

Apart from these costs, there is also a loss in production due to stand still of the rotor. The following stand still is assumed for the different control strategies, where a stand still of 1 day when inspected and a stand still of 2 days when repaired are assumed:

- Control strategy 1: 10 inspections and 9 repairs
- Control strategy 2: 10 inspections and 1 repairs
- Control strategy 3: 5 inspections and 0 repairs
- Control strategy 4: 5 inspections and 0 repairs
- Control strategy 5: 2 inspections and 0 repairs
- Control strategy 6: 2 inspections and 0 repairs

Based on these prices and costs, the cases in Table 4 to 8 are evaluated in the next section.

Wind Energ. Sci. Discuss., https://doi.org/10.5194/wes-2017-62
Manuscript under review for journal Wind Energ. Sci.
Discussion started: 21 February 2018

eawe european academy of wind energy
Open Access WIND ENERGY SCIENCE DISCUSSIONS

5.2 Results

Based on the assumption about the precipitation and the corresponding control, Table 4 to Table 8, the aerodynamic modeling and the cost of energy, inspection and repair, the overall cost of operation are calculated for the different control strategies. The energy production is computed by dividing the energy production over the life time into 10 different power curves. The power curve for the clean rotor is valid for the first 20th of the lifetime. The power curve with 10% of severe leading edge roughness is valid for the next 10th of the lifetime, the power curve with 20% of severe leading edge roughness is valid for the next 10th of the lifetime and so on. When the lifetime is reached, the turbine will operate with the most severe leading edge roughness until the next whole year has past, and then it will be repaired. E.g. with a life time of 1.6 years the rotor will be repaired after 2 years, because blade repairs are mainly carried out during the summer, when temperature, humidity and wind are sometimes appropriate. After repair, it is assumed that the blades are completely clean and that they are as wear-resistant as new blades. Besides the loss of energy production due to degradation in aerodynamic performance, the losses due to inspection and repair are also included. Also, the losses due to the reduction in maximum tip speed is included, where it is assumed that the duration of tip speed reduction is three times the time of the heavy precipitation event, because the turbine cannot react instantaneously. Thus, the loss of energy production and thereby of the income caused by both leading edge erosion and stand still due to inspection and repair are included.

In Fig. 15 AEP including stand still due to inspection and repair is reflected. It is seen, that applying control strategy 1, where there is no reduction of the maximum tip speed, the loss of AEP is significant with up to 3.5% compared to the reference case with no erosion and no inspections and repairs. The loss of AEP is clearly dependent on the wind climate. For low wind speed sites with A=7m/s the loss is greater than for sites with higher wind speeds, A=9m/s.

In Figure to Figure 7 the loss of income due to lost AEP, inspection and repair are seen with the assumption of different costs of energy, inspection and repair. From the plots it is seen, that the loss of income can be significant. The income is very dependent on the energy price and the cost of repair, but a clear trend is that the erosion safe mode increases the income. Even the very advanced erosion safe mode, control strategy 5, with rather low tip speeds results in a significant improvement. As an example, control strategy 2 can be investigated. Here, the tip speed is reduced from 90m/s to 70m/s during 5.4 hours/year and from 90m/s to 80m/s during 26.4 hours/year due to heavy precipitation. In this case AEP is increased with around 1% and the income loss is decreased from 15.4% to 4.5% in the worst case and from 4.7% to 2.7% in the best case, depending on assumptions in cost and wind climate.

Wind Energ. Sci. Discuss., https://doi.org/10.5194/wes-2017-62
Manuscript under review for journal Wind Energ. Sci.
Discussion started: 21 February 2018

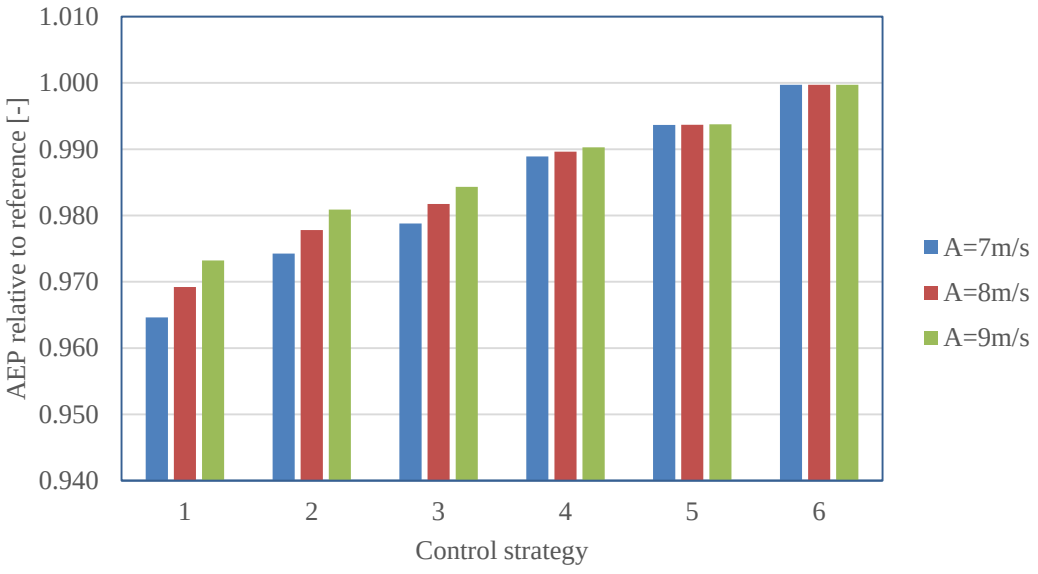

Figure 15: AEP relative to AEP with no erosion.

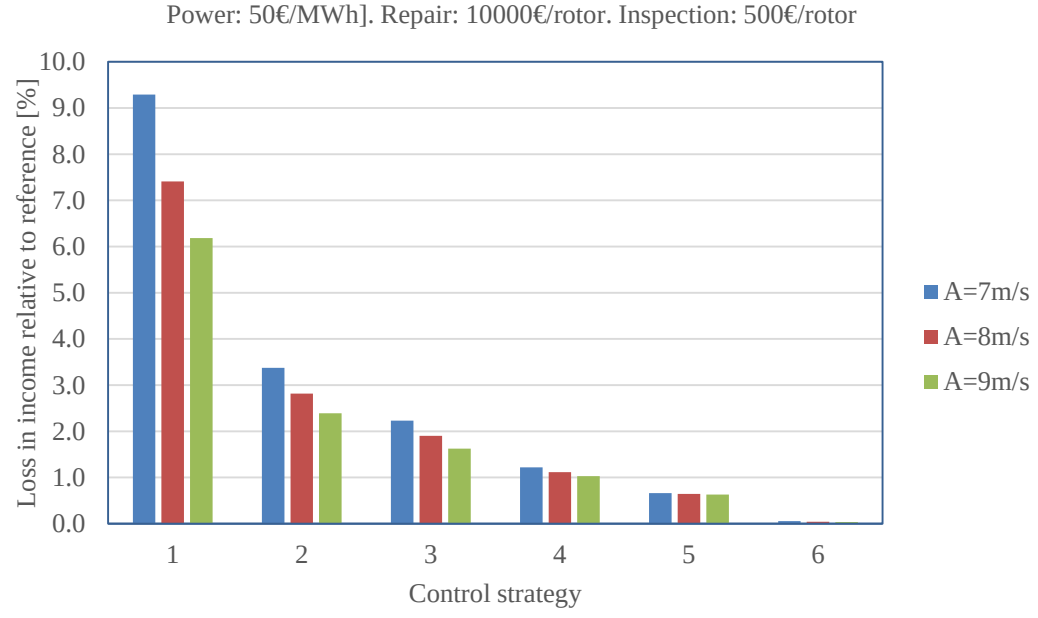

Figure 16: Loss of income due to erosion, inspection and repair. Power: 50€/MWh]. Repair: 10000€/rotor. Inspection: 500€/rotor.

Wind Energ. Sci. Discuss., https://doi.org/10.5194/wes-2017-62
Manuscript under review for journal Wind Energ. Sci.
Discussion started: 21 February 2018

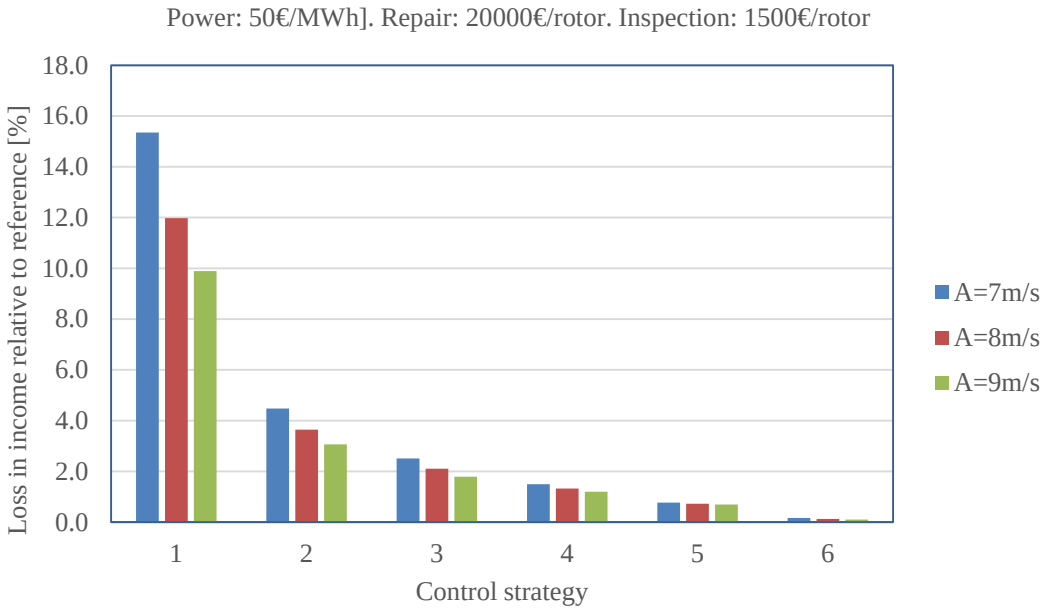

Figure 17: Loss of income due to erosion, inspection and repair. Power: 50€/MWh]. Repair: 20000€/rotor. Inspection: 1500€/rotor

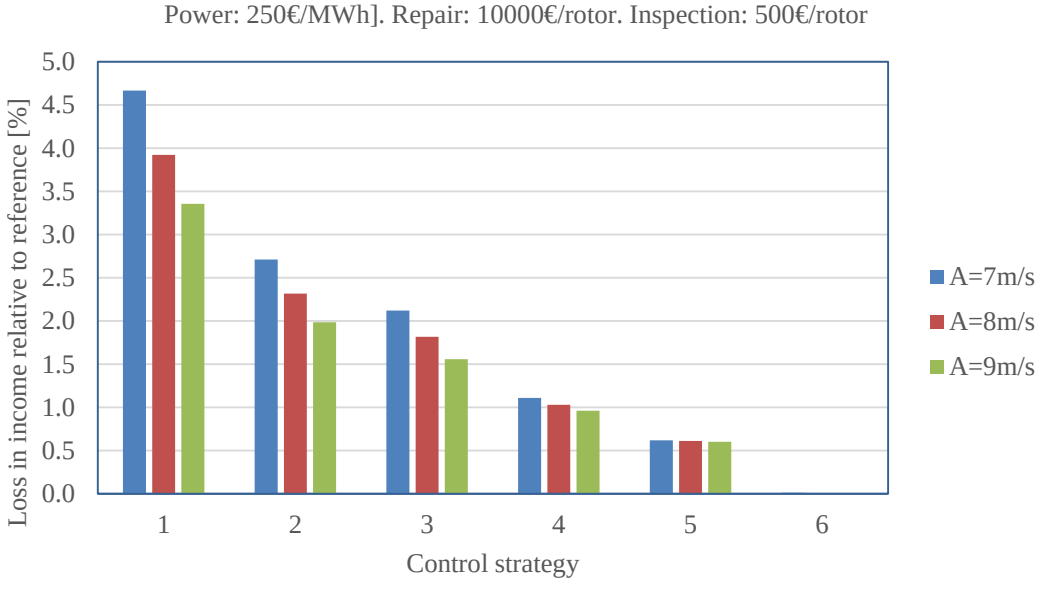

Figure 18: Loss of income due to erosion, inspection and repair. Power: 250€/MWh]. Repair: 10000€/rotor. Inspection: 500€/rotor.

Wind Energ. Sci. Discuss., https://doi.org/10.5194/wes-2017-62
Manuscript under review for journal Wind Energ. Sci.
Discussion started: 21 February 2018

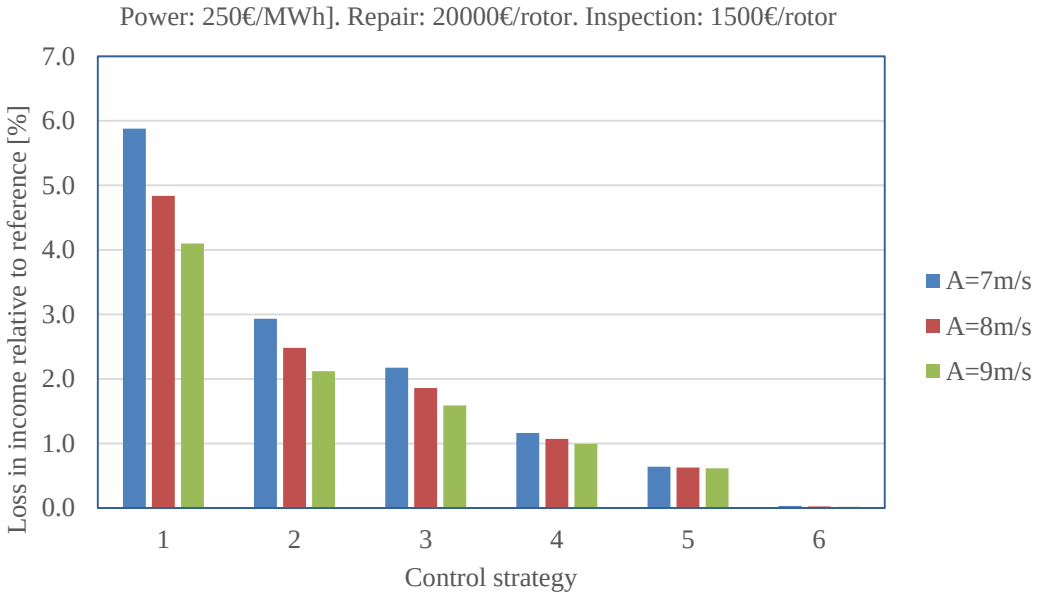

Figure 19: Loss of income due to erosion, inspection and repair. Power: 250€/MWh]. Repair: 20000€/rotor. Inspection: 1500€/rotor.

6 Discussion

This paper is a concept paper proposing a framework for prediction and mitigation of leading edge erosion. In order to demonstrate the concept quantitatively, a number of simplifying assumptions and approximations were made.

The assumption of homogenous droplet size for a given rain intensity is obviously an idealization of reality. For a given rain event the droplets sizes are distributed as explained in paragraph 4. These correlations may vary a lot between different types of precipitation, climates, temperatures, levels of pollution, etc. Still the median droplet size and the frequency of large droplets generally increase with increasing rain intensity.

The assumption that the damage increment scales with the kinetic energy, and that SN curve for one droplet size can be extrapolated to other droplet sizes as suggested in Sect. 3.2 may be controversial. However, there must be a strong correlation between the droplet diameter and the incremental damage. Particularly so for damage modes related to body waves propagating into the structure, affecting the material below the surface, like delamination and cracks in matrix, filler and top coats. It is obvious that small droplets affect only the material very close to the surface, whereas larger droplets and hail have the required kinetic energy and size of stress field to affect the structure below the surface. The droplet size is expected to be of particular importance for the modern type of leading edge protection, where coating of very tough and compliant elastomers is applied over the top coat to absorb the impact energy. Some of these materials seem to be extremely durable without any signs of Rayleigh wave induced surface cracks. But for high energy impacts they can still transfer enough energy to damage the underlying structure or to detach the elastomer coating from the top coat.

The correlation between droplet size and damage increment depends a lot on the material, leading edge configuration and failure mode. For surface cracking of brittle top coats the many impacts with smaller droplets may generate more accumulated damage than the few large droplets as suggested by Amirzadeh et al., (2017). However, for elastomeric protective coating the damage mode may be debonding from the top coat/gelcoat, and in this case it may be opposite.

The assumption that the aerodynamic performance decreases linearly with time is not necessarily true. Typically, there will be a long incubation period, where the surface roughness is nearly unaffected, and then the roughness increases at a high rate.

The correlation between leading edge damage and loss of aerodynamic performance is not fully understood. The loss depends a lot on the aerodynamic profile of the blade and other factors. However, simulations and wind tunnel tests have been carried out, where leading edge roughness has been investigated and quantified. The transfer function between life time and aerodynamic performance is not understood.

The costs for inspection and repair also vary quite a bit. They are, however reported to be significant these years, in particular for off shore turbines.

The erosion issue has become significant, as the tip speed has increased along with the development towards larger turbines. Many modern turbines have tip speeds at the order of 80 to 90 m/s. In order to reduce the shaft torque in future designs, it may be attractive to increase tips speeds even beyond 100 m/s. Then occasional tip speed reduction for erosion control will be even more important, even when stronger leading edge designs are developed.

The expenses for establishing erosion control are not assessed. These will relate to control algorithms on the turbine control software, precipitation sensors in each wind turbine park and connections between the sensor and each turbine.

As demonstrated in Sect. 5.2, the economic potential of erosion safe mode turbine control is significant. Even if the correlations between precipitation intensity and incremental damage or between degree of erosion and aerodynamic performance are not as strong as here assumed, the cost - benefit balance may still be in favor of erosion control.

7 Conclusions

A framework for prediction and a mitigation strategy for leading edge erosion was presented. The model takes into account the entire value chain: leading edge test data, actual on site precipitation, erosion rate, loss of production due to erosion, operation and maintenance.

The lost production due to occasional tip speed reduction is marginal in proportion to the alternative of lost production due to eroded blades. Thus, the cost – benefit balance of erosion control looks very promising and shows a great potential for reducing the loss of produced energy due to erosion and the cost of operation and maintenance.

To accomplish erosion control there is a need for more knowledge on the correlation between precipitation and erosion for different leading edge structures and materials, and for development of methods and equipment for on-site now casting of precipitation.

Data availability. Please contact the corresponding author.

Author contributions. JIB had the lead on paper writing, test data analysis and lifetime prediction. CBH contributed mainly on precipitation and CB mainly on wind turbine control. All contributed to writing the paper.

Competing interests. The authors declare that they have no conflict of interest.

Acknowledgements. The financial support from Innovation Fund Denmark (6154-00018B) for the project EROSION (www.rain-erosion.dk) is gratefully acknowledged. The authors want to acknowledge Polytech A/S for kindly providing the laboratory test specimen images. Permission to use the GPCP annual mean precipitation (Fig. 9) is kindly granted by Todd Mitchell.

References

Adler, W.F.: Rain impact retrospective and vision for the future, Wear, 233-235, 25-38, 1999.

Adler, W.F.: Waterdrop Impact Modeling. Wear, 186–187, 341–51, 1995.

Amirzadeh, B., Louhghalam, A., Raessi, M., and Tootkaboni, M.: A computational framework for the analysis of rain-induced erosion in wind turbine blades, part I: Stochastic rain texture model and drop impact simulations, Journal of Wind Engineering and Industrial Aerodynamics, 163:44-54, http://dx.doi.org/10.1016/j.jweia.2016.12.007 2017.

Amirzadeh, B., Louhghalam, A., Raessi, M., and Tootkaboni, M.: A computational framework for the analysis of rain-induced erosion in wind turbine blades, part II: Drop impact-induced stresses and blade coating fatigue life, Journal of Wind Engineering and Industrial Aerodynamics, 163:33-43, http://dx.doi.org/10.1016/j.jweia.2016.12.006 2017.

ASTM: ASTM G73 - Standard Test Method for Liquid Impingement Erosion Using Rotating Apparatus. Astm, 1–19, 2012.

Bak, C., Johansen, J., and Andersen, P.B.: Three-Dimensional Corrections of Airfoil Characteristics Based on Pressure Distributions. Proc. the European Wind Energy Conference & Exhibition (EWEC), 27. Feb. – 2. Mar. 2006, Athens, Greece, 2006.

Best, A. C.: The size of distribution of raindrops, Quart. J. R. Met. Soc., 76, p. 16, 1950.

Blowers, R. M.: On the Response of an Elastic Solid to Droplet Impact. IMA Journal of Applied Mathematics (Institute of Mathematics and Its Applications), 5(2), 167–93, 1969.

Bowden, F. P. B., and J. H. Brunton, J.H.:The Deformation of Solids by Liquid Impact at Supersonic Speeds. Proc. Roy .Soc., 263, 433–50, 1961.

Bowden, F. P., and Field, J.E.: The Brittle Fracture of Solids by Liquid Impact, by Solid Impact, and by Shock. Proceedings of the Royal Society A: Mathematical, Physical and Engineering Sciences, 282(1390), 331–52, 1964

Bringi, V. N., Chandrasekar, V., Hubbert, J., Gorgucci, E., Randeu, W. L., and Schoenhuber, M.: Raindrop size distribution in different climatic regimes from disdrometer and dual-polarized radar analysis, Journal of the Atmospheric Sciences, vol. 60, no. 2, pp. 354–365, https://doi.org/10.1175/1520-0469(2003)060<0354:RSDIDC>2.0.CO;2, 2003.

Brøndsted, P., Andersen, S.I., Lilholt, H. “Fatigue damage accumulation and lifetime prediction of GFRP materials under block loading and stochastic loading,” Proceedings, Polymer composites, Expanding the limits. 18th Risø Int. symposium, 1997

Cao, Y., Wu, Z., and Xu, Z.: Effects of rainfall on aircraft aerodynamics, Progress in Aerospace Sciences, Vol.71, p. 85-127, DOI: 10.1016/j.paerosci.2014.07.003 2014.

Climate-Charts.com http://www.climate-charts.com/World-Climate-Maps.html#rain (accessed Dec. 2017)

Cortés, E., Sánchez, F., O'Carroll, A. Madramany, B., Hardiman, M., and Young, T.M.: On the Material Characterisation of Wind Turbine Blade Coatings: The Effect of Interphase Coating-Laminate Adhesion on Rain Erosion Performance. Materials, 10(10), 2017.

Dear, J. P., and Field, J.E.: High-Speed Photography of Surface Geometry Effects in Liquid/solid Impact. Journal of Applied Physics, Review of Scientific Instruments, 63(10):1015–1650, 1988.

de Haller, P.:Untersuchungen Über Die Durch Kavitation Hervorgerufenen Korrosionen. Schweizerische Bauzeitung, 243, 1933.

DMI http://www.klimatilpasning.dk/viden-om/klima/klimaaendringeridanmark/aendringer-i-nedboer/nedboeren-i-danmark-fra-1874-til-i-dag.aspx (accessed Dec. 2017)

Drela, M.: XFOIL, An Analysis and Design System for Low Reynolds Number Airfoils. Low Reynolds Number Aerodynamics, vol. 54, In Springer.Verlag Lec. Notes in Eng., 1989.

Echtermeyer, A.T.: Fatigue of Glass Reinforced Composites Described by One Standard Fatigue Lifetime Curve, EWEA Conference, pp. 391-396, 1994.

Ellis, T. D., L'Ecuyer T., Haynes, J. M., and Stephens, G. L.: How often does it rain over the global oceans? The perspective from CloudSat, Geophys. Res. Lett., 36, L03815, doi:10.1029/2008GL036728, 2009.

ESDAC esdac.jrc.ec.europa.eu, European Commission, Joint Research Centre (accessed Dec. 2017)

Evans, A. G., Ito, Y. M., and Rosenblatt, M.: Impact damage thresholds in brittle materials impacted by water drops, J. Appl. Phys., vol. 51, no. 5, pp. 2473–2482, doi: http://dx.doi.org/10.1063/1.328021, 1980.

Fakhari, A., and Rahimian, M.H.: Simulation of Falling Droplet by the Lattice Boltzmann Method. Communications in Nonlinear Science and Numerical Simulation, 14(7), 3046–55, 2009.

FMI https://finland.fi/life-society/finlands-weather-and-light/ (accessed Dec. 2017)

Frich, P., Rosenørn, S., Madsen, H., and Jensen, J. J.: Observed precipitation in Denmark 1961-1990. Danish Meteorological Institute. Technical Report 97-8, Copenhagen, Denmark.

Fuglsang, P. and Thomsen, K.: Site-specific design optimization of 1.5-2.0 MW wind turbines. J. Solar Energy Eng. 123 , 296-303, 2001.

Fyall, A. A.: Meteorological parameters relevant to the phenomenon of rain erosion, First rain erosion conference, pp. 30–42, 1965.

Geiss, R.H., Rice, K.P., Keller, R.R., and Solin, J.: Methods for Comparing Fatigue Lives for Spectrum Loading. International Journal of Fatigue, 12(1), 35–42, 1990.

Gohardani, O.: Impact of erosion testing aspects on current and future flight conditions, Prog. Aerospace Sci. 47,280–303, https://doi.org/10.1016/j.paerosci.2011.04.001, 2011.

Gorgucci, E., Baldini, L., and Chandrasekar, V.: What Is the Shape of a Raindrop? An Answer from Radar Measurements. Journal of the Atmospheric Sciences, 63(11):3033–44, 2006.

GPCC http://www.gtn-h.info/about/the-network/gpcc/ (accessed Dec. 2017)

GPCP http://research.jisao.washington.edu/data_sets/gpcp/ (accessed Dec. 2017)

Haosheng, C. and Shihan, L.: Inelastic damages by stress wave on steel surface at the incubation stage of vibration cavitation erosion, Wear, vol. 266, no. 1–2, pp. 69–75, DOI: 10.1016/j.wear.2008.05.011, 2009.

Heymann, F. J.: High-Speed Impact between a Liquid Drop and a Solid Surface. Journal of Applied Physics, .40, 5113, 1969.

Hong, Y. L., Din, J., and Jong, S. L.:, Statistical and Physical Descriptions of Raindrop Size Distributions in Equatorial Malaysia from Disdrometer Observations, Advances in Meteorology, vol. 2015, Article ID 253730, pp. 14, http://dx.doi.org/10.1155/2015/253730, 2015.

IEC 61400-1, Wind turbines – Part 1: Design requirements, Edition 3.1, ISBN 978-2-8322-1525-8, 2014

Jones, D. M. A. and Sims, A. L.: Climatology of instantaneous rainfall rates, Journal of Applied Meteorology vol. 17, pp. 1135-1140, https://doi.org/10.1175/1520-0450(1978)017<1135:COIRR>2.0.CO;2, 1978.

Keegan, M. H., Nash, D. H., and Stack, M. M.: On erosion issues associated with the leading edge of wind turbine blades, J. Phys. D. Appl. Phys. vol. 46 no. 38, p. 383001, stacks.iop.org/JPhysD/46/383001 2013.

Kubilay, A., Derome, D., Blocken, B., and Carmeliet, J.: CFD simulation and validation of wind-driven rain on a building facade with an Eulerian multiphase model, Build. Environ., vol. 61, pp. 69–81, http://dx.doi.org/10.1016/j.buildenv.2012.12.005, 2013.

Liersch, J. and Michael., J.: Investigation of the Impact of Rain and Particle Erosion on Rotor Blade Aerodynamics with an Erosion Test Facility to Enhancing the Rotor Blade Performance and Durability. Journal of Physics: Conference Series, 524(Torque):12023, 2014.

Macdonald, H., Infield, D., Nash, D. H., and Stack, M. M.: Mapping hail meteorological observations for prediction of erosion in wind turbines, Wind Energ., 19: 777–784, DOI: 10.1002/we.1854, 2016

Mason, B. J. and Andrews, J. B.: Drop-size distributions from vaiours types of rain, Q.J.R. Meteorol. Soc., 86: 346–353, DOI: 10.1002/qj.49708636906, 1960.

Miner, M.: Cumulative Damage in Fatigue, J. Appl. Mech, 12 (3), A159-A164, 1945.

Nearing, M. A., Bradford, J. M., and Holtz, R. D.: Measurement of Force vs. Time Relations for Waterdrop Impact, Soil Science Society of America Journal, vol. 50, no. 6. p. 1532, doi: 10.2136/sssaj1986.03615995005000060030x,1986.

Met.nohttps://www.google.dk/search?q=annual+rainfall+norway&source=lnms&tbm=isch&sa=X&ved=0ahUKEwiI24Gr7PfUAhXlO5oKHft0AYAQ_AUIBigB&biw=1280&bih=610&dpr=1.5#imgrc=HaVIEUIAJXgzzM:&spf=1499453733523

Met Office http://www.metoffice.gov.uk/learning/rain/how-much-does-it-rain-in-the-uk (accessed Dec. 2017)

Naipal, V., Reick, C., Pongratz, J., and Van Oost, K.: Improving the global applicability of the RUSLE model – adjustment of the topographical and rainfall erosivity factors, Geosci. Model Dev., 8, pp. 2893-2913, https://doi.org/10.5194/gmd-8-2893-2015, 2015.

NASA https://pmm.nasa.gov/trmm. (accessed Dec. 2017)

Panagos, P., Ballabio, C., Borrelli, P., Meusburger, K., Klik, A., Rousseva, S., Tadic, M.P., Michaelides, S., Hrabalikova, M., Olsen, P., Aalto, J., Lakatos, M., Rymszewicz, A., Dumitrescu, A., BeguerÃa, S., and Alewell, C.: Rainfall erosivity in Europe, Science of the Total Environment 511: 801-814. DOI: 10.1016/j.scitotenv.2015.01.008, 2015.

Panagos, P., Borrelli, P., Meusburger, K., Yu, B., Klik, A., Lim, K. J, Yang, J. A., Ni, J., Miao, C., Chattopadhyay,N., Sadeghi, S. H., Hazbavi, Z., Zabihi, M., Larionov, G. A., Krasnov, S. F., Gorobets, A. V., Levi, Y., Erpul, G., Birkel, C., Hoyos, N., Naipal, V., Oliveira, P. T. S., Bonilla, C.A., Meddi, M., Nel, W., Dashti, H. A., Boni, M., Diodato, N., Van Oost, K., Nearing, M., and Ballabio, C.: Global rainfall erosivity assessment
based on high-temporal resolution rainfall records, Scientific Reports, 7: 4175, DOI:10.1038/s41598-017-04282-8, 2017.

Peel, M. C., Finlayson, B. L., and McMahon, T. A.: Updated world map of the Köppen-Geiger climate classification, Hydrology and Earth System Sciences Discussions, European Geosciences Union, 11 (5), pp. 1633-1644, https://doi.org/10.5194/hess-11-1633-2007, 2007.

Poulsen, T., Hasager, C.B., Jensen, and C. M: The Role of Logistics in Practical Levelized Cost of Energy Reduction Implementation and Government Sponsored Cost Reduction Studies: Day and Night in Offshore Wind Operations and Maintenance Logistics, Energies 10(4), 464; doi:10.3390/en10040464, 2017.

Prayogo, G., Homma, H., Soemardi, T.P., and Danadorno, A. S.: Impact Fatigue Damage of GFRP Materials Due to Repeated Raindrop Collisions, Trans Indian Inst Met, 64: 501, DOI 10.1007/s12666-011-0078-5, 2011.

Ronold, K. and Echtermeyer, A.: Estimation composite of fatigue laminates curves for design of composite laminates, Compos. Part A Appl. Sci. Manuf., vol. 27, no. 6, pp. 485–491, DOI: 10.1016/1359-835X(95)00068, 1996.

Sanada, T., Ando, K., Colonius, T., A Computational Study of High-Speed Droplet Impact, FDMP, vol.7, no. 4, pp. 329-340, 2011,

Slot, H. M., Gelinck, E. R. M., Rentrop, C., and van der Heide, E.: Leading edge erosion of coated wind turbine blades: Review of coating life models, Renewable Energy 80, 737-848, http://dx.doi.org/10.1016/j.renene.2015.02.036, 2015.

SMHI http://www-markinfo.slu.se/eng/climate/ned.html (accessed Dec. 2017)

Smith, J. A., Hui, E., Steiner, M., Baeck, M. L., Krajewski, W. F., and Ntelekos, A. A.: Variability of rainfall rate and raindrop size distributions in heavy rain, Water Resour. Res., vol. 45, no. 4, pp. 1–12, DOI: 10.1029/2008WR006840, 2009.

Solin, J.: Methods for comparing fatigue lives for spectrum loading, Int. J. Fatigue, vol. 12, no. 1, pp. 35–42, https://doi.org/10.1108/17579861111135888, 1990.

Springer, G., Yang, C., Larsen, P.: Analysis of Rain Erosion of Coated Materials, Journal of Composite Materials, vol. 8, pp. 229-252, 1974.

Springer, G., Yang, C., Larsen, P.: Model for the rain erosion of fiber reinforced composites, AIAA journal, vol. 13, no. 7, pp. 877-883, 1975

Stephenson, S.: Wind blade repair: Panning, safety, flexibility, Composites World, 2011.

Wittrup, S.: Dong og Siemens giver Horns Rev 2 storstilet vinge-makeover, Ingeniøren, 2015. (In Danish)

Wobben, A.: Patent US2003/0165379 https://www.google.com/patents/US20030165379.

Woods, R. D.: Screening of Surface Wave in Soils, Journal of the Soil Mechanics and Foundations Division, Vol. 94, Issue 4, Pg. 951-980, 1968.

World Atlas http://www.worldatlas.com/articles/the-ten-wettest-places-in-the-world.html (accessed Dec. 2017)

WorldClim https://dasgeographer.wordpress.com/2013/09/05/world-precipitation-patterns/ (accessed Dec. 2017)

Zidane, I. F., Saqr, K. M., Swadener, G., Ma, X., and Shehadeh, M. F.: On the role of surface roughness in the aerodynamic performance and energy conversion of horizontal wind turbine blades: a review, Int. J. Energy Res., 40, 2054–2077, DOI: 10.1002/er.3580, 2016.